Mineralogical Magazine, October 2013, Vol. 77(7), pp. 2955–2974

Veblenite, $K_2\square_2Na(Fe^{2+}_5Fe^{3+}_4Mn^{2+}_7\square)Nb_3Ti(Si_2O_7)_2(Si_8O_{22})_2O_6(OH)_{10}(H_2O)_3$, a new mineral from Seal Lake, Newfoundland and Labrador: mineral description, crystal structure, and a new veblenite Si_8O_{22} ribbon

F. Cámara[1,2,3]*, E. Sokolova[3], F. C. Hawthorne[3], R. Rowe[4], J. D. Grice[4] and K. T. Tait[5]

[1] Dipartimento di Scienze della Terra, Università degli Studi di Torino, via Valperga Caluso 35, 10125 Torino, Italy
[2] CrisDi, Interdepartmental Centre for the Research and Development of Crystallography, Via P. Giuria 5, I-10125, Torino, Italy
[3] Department of Geological Sciences, University of Manitoba, 240 Wallace Building, 125 Dysart Road, Winnipeg, Manitoba R3T 2N2, Canada
[4] Research Division, Canadian Museum of Nature, 240 McLeod St, Ottawa, ON K1P 6P4, Ontario, Canada
[5] Department of Natural History, Royal Ontario Museum, 100 Queens Park, Toronto, ON M5S 2C6, Ontario Canada

[*Received 22 June 2013; Accepted 18 August 2013; Associate Editor: G.D. Gatta*]

ABSTRACT

Veblenite, ideally $K_2\square_2Na(Fe^{2+}_5Fe^{3+}_4Mn^{2+}_7\square)Nb_3Ti(Si_2O_7)_2(Si_8O_{22})_2O_6(OH)_{10}(H_2O)_3$, is a new mineral with no natural or synthetic analogues. The mineral occurs at Ten Mile Lake, Seal Lake area, Newfoundland and Labrador (Canada), in a band of paragneiss consisting chiefly of albite and arfvedsonite. Veblenite occurs as red brown single laths and fibres included in feldspar. Associated minerals are niobophyllite, albite, arfvedsonite, aegirine-augite, barylite, eudidymite, neptunite, Mn-rich pectolite, pyrochlore, sphalerite and galena. Veblenite has perfect cleavage on {001} and splintery fracture. Its calculated density is 3.046 g cm^{-3}. Veblenite is biaxial negative with α 1.676(2), β 1.688(2), γ 1.692(2) (λ 590 nm), $2V_{meas}$ = 65(1)º, $2V_{calc}$ = 59.6º, with no discernible dispersion. It is pleochroic in the following pattern: *X* = black, *Y* = black, *Z* = orange-brown. The mineral is red-brown with a vitreous, translucent lustre and very pale brown streak. It does not fluoresce under short and long-wave UV-light. Veblenite is triclicnic, space group $P\bar{1}$, *a* 5.3761(3), *b* 27.5062(11), *c* 18.6972(9) Å, α 140.301(3), β 93.033(3), γ 95.664(3)º, *V* = 1720.96(14) Å^3. The strongest lines in the X-ray powder diffraction pattern [*d*(Å)(I)(*hkl*)] are: 16.894(100)(010), 18.204(23)(0$\bar{1}$1), 4.271(9)(1$\bar{4}$1, 040, 120), 11.661(8)(001), 2.721(3)(1$\bar{9}$5), 4.404(3)($\bar{1}\bar{3}$2, 1$\bar{4}$2), 4.056(3)(031, 1$\bar{1}$2; 1$\bar{5}$2, $\bar{1}\bar{4}$3), 3.891(2)(003).

The chemical composition of veblenite from a combination of electron microprobe analysis and structural determination for H_2O and the Fe^{2+}/Fe^{3+} ratio is Nb_2O_5 11.69, TiO_2 2.26, SiO_2 35.71, Al_2O_3 0.60, Fe_2O_3 10.40, FeO 11.58, MnO 12.84, ZnO 0.36, MgO 0.08, BaO 1.31, SrO 0.09, CaO 1.49, Cs_2O 0.30, K_2O 1.78, Na_2O 0.68, H_2O 4.39, F 0.22, O = F −0.09, sum 95.69 wt.%. The empirical formula [based on 20 (Al+Si) p.f.u. is $(K_{0.53}Ba_{0.28}Sr_{0.03}\square_{0.16})_{\Sigma1}(K_{0.72}Cs_{0.07}\square_{1.21})_{\Sigma2}(Na_{0.72}Ca_{0.17}\square_{1.11})_{\Sigma2}(Fe^{2+}_{5.32}Fe^{3+}_{4.13}Mn^{2+}_{5.97}Ca_{0.70}Zn_{0.15}Mg_{0.07}\square_{0.66})_{\Sigma17}(Nb_{2.90}Ti_{0.93}Fe^{3+}_{0.17})_{\Sigma4}(Si_{19.61}Al_{0.39})_{\Sigma20}O_{77.01}H_{16.08}F_{0.38}$. The simplified formula is $(K,Ba,\square)_3(\square,Na)_2(Fe^{2+},Fe^{3+},Mn^{2+})_{17}(Nb,Ti)_4(Si_2O_7)_2(Si_8O_{22})_2O_6(OH)_{10}(H_2O)_3$. The infrared spectrum of the mineral contains the following bands (cm^{-1}): 453, 531, 550, 654 and 958, with shoulders at 1070, 1031 and 908. A broad absorption was observed between ~3610 and 3300 with a maximum at ~3525. The crystal structure was solved by

* E-mail: fernando.camaraartigas@unito.it
DOI: 10.1180/minmag.2013.077.7.06

© *2013 The Mineralogical Society*

direct methods and refined to an R_1 index of 9.1%. In veblenite, the main structural unit is an HOH layer, which consists of the octahedral (O) and two heteropolyhedral (H) sheets. The H sheet is composed of Si_2O_7 groups, veblenite Si_8O_{22} ribbons and Nb-dominant D octahedra. This is the first occurrence of an eight-membered Si_8O_{22} ribbon in a mineral crystal structure. In the O sheet, (Fe^{2+}, Fe^{3+}, Mn^{2+}) octahedra share common edges to form a modulated O sheet parallel to (001). HOH layers connect *via* common vertices of D octahedra and cations at the interstitial A(1,2) and B sites. In the intermediate space between two adjacent HOH layers, the A(1) site is occupied mainly by K; the A(2) site is partly occupied by K and H_2O groups, the B site is partly occupied by Na. The crystal structure of veblenite is related to several HOH structures: jinshanjiangite, niobophyllite (astrophyllite group) and nafertisite. The mineral is named in honour of David R. Veblen in recognition of his outstanding contributions to the fields of mineralogy and crystallography.

Keywords: veblenite, new mineral, Seal Lake, Newfoundland and Labrador, Canada, electron-microprobe analysis, crystal structure, veblenite ribbon, nafertisite, niobophyllite, jinshanjiangite.

Introduction

During recent work on astrophylite-group minerals (Cámara *et al.*, 2010), the holotype sample of niobophyllite #M26148 (Royal Ontario Museum, Toronto, Canada) was studied and in that sample we observed red brown single laths included in albite. The shape suggested that these laths were a distinct phase. A test on the diffractometer on one of the longer laths (<200 μm) gave unit-cell dimensions unknown for HOH *heterophyllosilicates* (Ferraris *et al.*, 1996; Ferraris, 2008). *Heterophyllosilicates* are related to TOT silicates: in *heterophyllosilicates*, five- to six-coordinated Ti(Nb) periodically substitute a row of silicate tetrahedra in the tetrahedral (T) sheets of a TOT layer, producing a heteropolyhedral (H) sheet, while the octahedral O sheet is maintained the same. In *heterophyllosilicates*, HOH layers can link directly or contain interstitial atoms between HOH layers. A single crystal X-ray diffraction study revealed that this is a new structure type with no analogues. Here we describe the properties and the structure of this new mineral.

The name is in honour of David R. Veblen (*b*. 1947, Minneapolis, Minnesota, USA) in recognition of his outstanding contributions to the fields of mineralogy and crystallography. He has established himself as one of the foremost experts in the use of TEM in geology and has made a significant contribution to the polysomatic approach in mineralogy. The new mineral species and its name have been approved by the Commission on New Minerals, Nomenclature and Classification of the International Mineralogical Association (IMA 2010-050). The holotype specimen of veblenite (the same as that of niobophyllite) is under catalogue number #M26148 at the Royal Ontario Museum, 100 Queen's Park, Toronto, Ontario M5S 2C6.

Occurrence and associated minerals

The mineral occurs at Ten Mile Lake, Seal Lake area, Newfoundland and Labrador (Canada) (latitude 54º12′N, longitude 62º30′W). It occurs as red brown single laths and fibres included in feldspar, in a band of paragneiss consisting chiefly of albite and arfvedsonite. The geology of the area has been interpreted in terms of a series of interbedded volcanic rocks and gneisses intruded by an alkaline syenite. Associated minerals are niobophyllite, albite, arfvedsonite, aegirine-augite, barylite, eudidymite, neptunite, Mn-rich pectolite, pyrochlore, sphalerite and galena (Nickel *et al.*, 1964 and references therein).

Physical and optical properties

The main properties of veblenite are presented in Table 1, where they are compared to those of jinshanjiangite, niobophyllite, and nafertisite. The mineral forms laths and fibres; the laths are hundreds of microns long and no more than tens of microns thick and wide (Fig. 1). Veblenite is red-brown, with a very pale brown streak and a vitreous lustre. The mineral is translucent. It has a perfect {001} cleavage, with splintery fracture. No parting was observed. It is not fluorescent under 240−400 nm ultraviolet radiation. The density of the mineral and the Mohs hardness could not be measured owing to the very small thickness of the flakes. Its calculated density (using the empirical formula) is 3.046 g cm^{-3}. The mineral is biaxial negative with α 1.676,

TABLE 1. Comparison of veblenite, jinshajiangite, niobophyllite and nafertisite.

Mineral	Veblenite	Jinshajiangite	Niobophyllite	Nafertisite
Reference*	(1)	(4, 8)	(2, 6, 7)	(3, 5)
Formula	$K_2\square_2Na(Fe^{2+}_5Fe^{3+}_4Mn_7)Nb_3Ti(Si_2O_7)_2(Si_8O_{22})_2O_6(OH)_{10}(H_2O)_3$	$Ba_2Na_2Fe^{2+}_8Ti_4(Si_2O_7)_4O_4(OH,F)_6$	$K_2NaFe^{2+}_7(Nb,Ti)(Si_4O_{12})_2O_2(OH)_4(O,OH)$	$(Na,K)_3(Fe^{2,3+}\square)_{10}Ti_2(Si_6O_{17})_2O_3(OH,O)_6$
System	Triclinic	Monoclinic	Triclinic	Monoclinic
Space group	$P\bar{1}$	$C2/m$	$P\bar{1}$	$A2/m$
a (Å)	5.3761	10.6785	5.4022	5.353
b	27.506	13.786	11.8844	16.18
c	18.6972	20.700	11.6717	21.95
α (°)	140.301	90	112.990	90
β	93.033	94.937	94.588	94.6
γ	95.664	90	103.166	90
V (Å^3)	1720.96	3035.93	659.7	1894.41
Z	1	4	1	2
D_{calc} (g cm^{-3})	3.046	3.767	3.406	2.83
D_{meas} (g cm^{-3})	n.d.	3.61	3.42	2.7
Strongest lines in the powder pattern, d_{obs} (Å) (I)	16.894 (100)	3.44 (100)	3.506 (100)	10.94 (100)
	18.20 (23)	3.15 (80)	10.52 (90)	13.00 (30)
	4.27 (9)	2.630 (80)	2.778 (80)	2.728 (25)
	11.66 (8)	2.570 (80)	2.574 (70)	2.641 (20)
	2.72 (3)	10.2 (70)	3.019 (60)	2.547 (15)
	4.40 (3)	1.715 (50 broad)	3.258 (50)	2.480 (15)
	4.06 (3)	2.202 (40)	2.475 (40)	3.638 (10)
Optical class (sign)	biaxial (−)	biaxial (+)	biaxial (−)	biaxial (−)
α (589.3 nm)	1.676(2)	1.792	1.724	1.627
β	1.688(2)	1.801	1.760	1.667
γ	1.692(2)	1.852	1.772	1.693
$2V_{meas}$ (°)	65.3(1.2)	72	60	75(2)
$2V_{calc}$ (°)	59.6	46.6	59	76

* Jinshajiangite: formula, unit-cell parameters, space group and calculated density (8); powder pattern, D_{meas} and optics (4); Niobophyllite: formula (7); unit-cell parameters, space group and calculated density (2); D_{meas}, powder pattern and optics (6); Nafertisite: formula, unit-cell parameters, space group and calculated density (3); D_{meas}, powder pattern and optics (5). n.d. = not determined.

References: (1) this work; (2) Cámara *et al.* (2010); (3) Ferraris *et al.* (1996); (4) Hong and Fu (1982); (5) Khomyakov *et al.* (1995); (6) Nickel *et al.* (1964); (7) Sokolova (2012); (8) Sokolova *et al.* (2009).

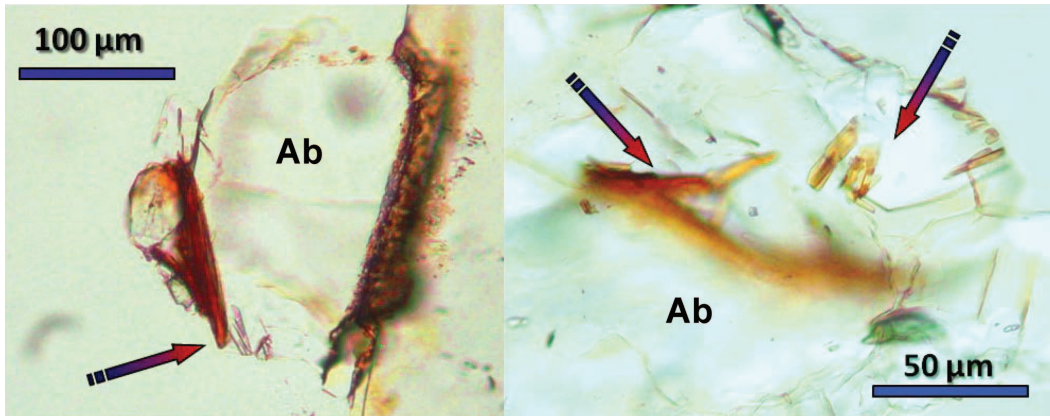

FIG. 1. Images of veblenite crystals (marked with arrows) in an albite (ab) matrix in probe mounting.

β 1.688, γ 1.692 (λ 590 nm), all ±0.002, $2V_{meas.}$ = 65.3(1.2)º, $2V_{calc.}$ = 59.6º, with no determined dispersion. Optical orientation is

	a	*b*	*c*
X	87.8º	92.3º	126.7º
Y	96.0º	168.2º	36.9º
Z	173.6º	78.5º	93.0º

It is pleochroic with *X* = black, *Y* = black, *Z* = orange-brown. A Gladston-Dale compatibility index of 0.025 is rated as excellent.

The infrared powder absorption spectrum was recorded using a Nicolet FTIR 740 spectrophotometer in the range 4000−400 cm^{-1} (Fig. 2). In the principal OH-stretching region (3800−3000 cm^{-1}), the spectrum shows a broad absorption between ~3610 and ~3300 cm^{-1} with a maximum at ~3525 cm^{-1} in accord with the presence of several OH and H_2O groups in the structure. Several weak bands between 3000 and 2000 cm^{-1} and weak bands at 1480 and 1377 cm^{-1} are due to glue that was used during transport of the crystals and subsequently could not be completely removed from the very delicate crystals. There is a band at 1637 cm^{-1} due to the H−O−H bend of H_2O groups in the structure. There is a sharp intense band at 958 with shoulders at 1070, 1031 and 908 cm^{-1} due to the various stretching modes of the SiO_4 group, and weaker bands at 654, 550, 531 and 453 cm^{-1} due to complex lattice modes involving the octahedra and coupled motions between the various polyhedra.

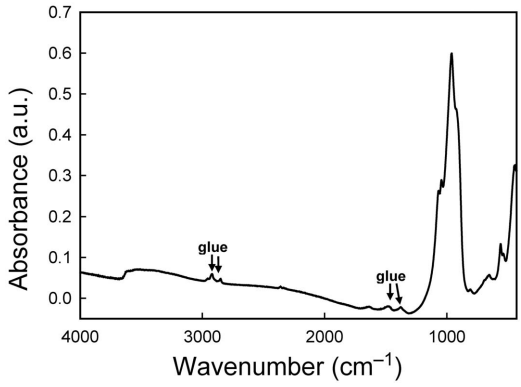

FIG. 2. IR spectrum of veblenite.

Chemical composition

The chemical composition of veblenite was determined with a Cameca SX-100 electron-microprobe in wavelength-dispersion mode with an accelerating voltage of 15 kV, a specimen current of 20 nA, a beam size of 10 µm and count times on peak and background of 20 and 10 s, respectively. The following standards were used: $Ba_2NaNb_5O_{15}$ (Ba, Nb), $SrTiO_3$ (Sr), titanite (Ti), diopside (Si, Ca), andalusite (Al), fayalite (Fe), spessartine (Mn), forsterite (Mg), gahnite (Zn) orthoclase (K), albite (Na), pollucite (Cs) and F-bearing riebeckite (F). Sn, Zr, Ta, Pb and Rb were sought but not detected; Li and Be were sought by LA-ICP-MS but not detected. Data were reduced using the PAP procedure of Pouchou and Pichoir (1985). H_2O and the Fe^{3+}/Fe^{2+} ratio were calculated from structure refinement. The low total of ~96 wt.% is due to the thinness of the crystal. We did not have material sufficient for direct

determination of H_2O, but the presence of H_2O was confirmed by infrared spectroscopy (see above). The chemical composition of veblenite is given in Table 2. The empirical formula (based on Si + Al = 20 atoms p.f.u.) is $(K_{0.53}Ba_{0.28}Sr_{0.03}\square_{0.16})_{\Sigma1}(K_{0.72}Cs_{0.07}\square_{1.21})_{\Sigma2}(Na_{0.72}Ca_{0.17}\square_{1.11})_{\Sigma2}(Fe^{2+}_{5.32}Fe^{3+}_{4.13}Mn^{2+}_{5.97}Ca_{0.70}Zn_{0.15}Mg_{0.07}\square_{0.66})_{\Sigma17}(Nb_{2.90}Ti_{0.93}Fe^{3+}_{0.17})_{\Sigma4}(Si_{19.61}Al_{0.39})_{\Sigma20}O_{77.01}H_{16.08}F_{0.38}$, $Z = 1$.

X-ray powder diffraction

The powder-diffraction pattern for veblenite was recorded at the Canadian Museum of Nature using a Bruker D8 Discover micro-powder diffractometer with a Hi-Star multi-wire 2D detector at 12 cm, calibrated following Rowe (2009) and using a pseudogandolfi approach. Table 3 shows the X-ray powder-diffraction data (for Cu$K\alpha$, λ = 1.54178 Å; 40 kV/40 mA) with refined unit-cell dimensions; the latter are in close agreement with corresponding values determined by single-crystal diffraction (Table 4).

Crystal structure

X-ray data collection and structure refinement

X-ray diffraction data for the single crystal of veblenite were collected with a Bruker P4 diffractometer with a CCD 4K Smart detector (Mo$K\alpha$ radiation) using the largest crystal found in the sample included in a feldspar grain, extracted using a razor blade to open the grain; the crystal came off free of matrix (no additional spots were observed in the diffraction images). The intensities of the 25883 reflections were recorded using a 0.2º frame and an integration time of 60 s; 15845 are unique (R_{int} = 9.47%). An empirical absorption correction (*SADABS*, Sheldrick, 2008) was applied. Only reflections with $-5 < h < 5$, $-30 < k < 30$, $-20 < l < 20$, i.e. 46º 2θ, corresponding to 4777 unique reflections R_{int} = 6.66% were used for refinement. The refined unit-cell parameters were obtained from 7614 reflections with $I > 10\sigma I$ (Table 4). The crystal structure of veblenite was solved in space group $P\bar{1}$ by direct methods using *SHELXS* (Sheldrick, 2008) and refined with the Bruker *SHELXTL Version 5.1* system of programs (Sheldrick, 2008). The crystal structure contains 3 groups of cation sites: *D* and *Si* sites of the H sheet, *M* sites of the O sheet, and interstitial *A* and *B* sites; site labelling is in accord with TS-block minerals (Sokolova, 2006) and astrophyllite-group minerals (Sokolova, 2012). Because of the small size of the single crystal, it was not possible to collect enough reflections for a full anisotropic refinement. Therefore displacement parameters were refined anisotropically only for atoms of the O sheet, D and Si atoms of H sheets and interstitial atoms. The occupancies of cations at the *M*(1)–*M*(6) sites were fixed (scattering curve of Fe) while those at the *D*(1A)–*D*(2B) and *M*(7)–*M*(9) sites were refined. The observed scattering at the *M*(7)–*M*(9) sites was held fixed in the last cycles of refinement (scattering curve of Mn). Occupancies of atoms were also refined

TABLE 2. Chemical composition and unit formula* for veblenite.

Oxide	Wt.%	Formula unit	a.p.f.u.
Nb_2O_5	11.69	Si	19.61
TiO_2	2.26	Al	0.39
SiO_2	35.71	Σ	20
Al_2O_3	0.60		
Fe_2O_3**	10.40	Fe^{2+}	5.32
FeO**	11.58	Fe^{3+}	4.13
MnO	12.84	Mn^{2+}	5.97
ZnO	0.36	Ca	0.70
MgO	0.08	Zn	0.15
BaO	1.31	Mg	0.07
SrO	0.09	Σ17M	16.34
CaO	1.49		
Cs_2O	0.30	Nb	2.90
K_2O	1.78	Ti	0.93
Na_2O	0.68	Fe^{3+}	0.17
H_2O**	4.39	Σ4D	4.00
F	0.22		
$-O=F_2$	0.09	Na	0.72
Total	95.69	Ca	0.17
		Σ B	0.89
		K	1.25
		Ba	0.28
		Cs	0.07
		Sr	0.03
		Σ3A	1.63
		F	0.38
		OH	9.62
		Σ	10.00
		H_2O	3.23

* calculated on cation basis: Si + Al = 20 a.p.f.u.;
** calculated from structure solution and refinement: FeO(total) = 20.94 wt.%; OH + F = 10 p.f.u., H_2O = 3.23 p.f.u.

TABLE 3. X-ray powder diffraction data for veblenite.*

$I_{obs.}$	d_{obs} (Å)	d_{calc} (Å)	I_{calc}	h	k	l
22.7	18.204	18.382	75	0	$\bar{1}$	1
100	16.894	17.094	66	0	1	0
7.8	11.661	11.671	100	0	0	1
2.8	4.404	4.444	5	$\bar{1}$	$\bar{3}$	2
		4.404	3	1	$\bar{4}$	2
8.7	4.271	4.304	1	1	$\bar{4}$	1
		4.274	1.5	0	4	0
		4.097	1	1	2	0
2.7	4.056	4.031	1	0	3	1
		4.022	1	1	$\bar{1}$	2
		4.021	2	1	$\bar{4}$	2
		3.996	1	$\bar{1}$	$\bar{4}$	3
2.4	3.891	3.890	4	0	0	3
1.6	3.747	3.750	3	$\bar{1}$	4	0
1.6	3.340	3.340	7	0	$\bar{1}$	4
2.3	3.284	3.281	7	0	1	3
1.4	3.007	3.014	2	$\bar{1}$	$\bar{7}$	4
		3.009	2	1	$\bar{8}$	4
		3.009	2	1	4	0
2.9	2.721	2.721	6	1	$\bar{9}$	5
		2.720	6	$\bar{1}$	$\bar{8}$	4
2.2	2.627	2.628	2	$\bar{1}$	$\bar{7}$	2
		2.618	2	1	$\bar{8}$	6
2.1	2.557	2.562	4	1	$\bar{9}$	6
		2.557	4	$\bar{1}$	$\bar{8}$	3
1.3	2.324	2.329	1	1	$\bar{9}$	7
		2.322	1	$\bar{1}$	$\bar{8}$	2
1.9	2.163	2.152	1	1	$\bar{1}0$	2
1.9	2.072	2.074	0.5	$\bar{1}$	$\bar{8}$	1
		2.072	0.5	$\bar{1}$	$\bar{9}$	2
1.5	2.046	2.049	1	1	7	0
		2.041	1	1	$\bar{8}$	8
1.8	1.8666	1.8659	0.5	1	$\bar{1}0$	2
		1.8638	0.5	$\bar{1}$	$\bar{9}$	1
1.2	1.7533	1.7534	1	1	6	2

* Indexed on a = 5.41(3), b = 27.36(5), c = 18.62(3) Å, α = 140.17(8), β = 93.3(2), γ = 95.6(1)º, V = 1719(6) Å^3; d_{calc}, I_{calc} and hkl values are from the powder pattern calculated from single-crystal data.

for the interstitial $A(1)$ site (scattering curve of Ba), $A(2A)-A(2D)$ sites (scattering curve of K), B site (scattering curve of Na), and for anion sites [$W(1)-W(5)$], corresponding to interstitial H_2O groups, with U_{iso} fixed at 0.05 Å^2. The structure model was refined to an R_1 value of 9.05%.

At the last stages of the refinement, three peaks with magnitudes of ~1.5 e Å^{-3} were found as satellites of the $M(1)$, $M(6)$ and $M(9)$ sites. Occupancies of atoms at these subsidiary peaks were refined with the scattering curves of Fe, Fe and Mn, respectively, and with U_{iso} fixed at 0.01 Å^2. Refined occupancies of these subsidiary peaks vary from 2 to 5%. Scattering curves for neutral atoms were taken from the International Tables for Crystallography (Wilson, 1992). The unusual cell setting chosen for the structure (Tables 1, 3 and 4) is obtained from the reduced cell a = 5.3761(3), b = 17.7419(10), c = 18.6972(11) Å, α = 97.991(1), β = 93.032(2), γ = 102.050(1)º *via* the transformation (1,0,0|0,1,−1|0,0,1). The chosen setting with a large α is preferred in order to compare the structure topology of veblenite with those of jinshajiangite and niobophyllite. Details of data collection and structure refinement are given in Table 4, final atom parameters are given in Table 5, selected interatomic distances in Table 6, refined site-scattering values and assigned populations for selected cation sites are given in Table 7, and bond valences in Table 8 (bond-valence parameters from Brown, 1981). Tables of structure factors and anisotropic displacement parameters for several atoms have been deposited with the Principal Editor of *Mineralogical Magazine* and are available from www.minersoc.org/pages/e_journals/dep_mat_mm.html.

Site-population assignment

As we did not have enough material to determine the Fe^{3+}/Fe^{2+} ratio directly by Mössbauer spectroscopy, the Fe^{3+}/Fe^{2+} ratio was calculated from the M−O distances of the M(1−9) octahedra of the O sheet; minor Fe^{3+} was added to fill (Nb,Ti)-dominant D sites. Consider first the two (Nb,Ti)-dominant $D(1,2)$ sites in the H sheet. Each D site is split in two sites: $D(1A)$ and $D(1B)$, and $D(2A)$ and $D(2B)$. We assign cations to these sites assuming 50% occupancy for each split site. The split site is related to a different charge arrangement: $D(1A)$ and $D2(B)$ sites are closer to the O sheet and have a lower charge, while $D(1B)$ and $D(2A)$ sites are further from the O sheet and are almost fully occupied by Nb. Total Nb + Ti is < 4 a.p.f.u. Thus we assign Fe^{3+} to achieve 100% occupancy of the D sites. The resulting calculated site-scattering is significantly lower than the aggregate refined scattering at these sites (141.19 *vs.* 153.42 electrons per formula unit (e.p.f.u.), Table 7), indicating heavier atom composition, although the chemical analyses confirmed the absence of Sn and Ta. We

TABLE 4. Miscellaneous refinement data for veblenite.

a (Å)	5.3761(3)
b	27.506(1)
c	18.697(1)
α (°)	140.301(2)
β	93.032(1)
γ	95.664(3)
V (Å^3)	1720.96(14)
Space group	$P\bar{1}$
Z	1
Absorption coefficient (mm^{-1})	4.47
F(000)	1527.0
$D_{calc.}$ (g/cm^3)	3.046
Crystal size (mm)	0.20 × 0.04 × 0.02
Radiation/filter	Mo$K\alpha$/graphite
$2\theta_{max}$ for structure refinement (°)	46.00
R_{int} (%)	6.65
Reflections collected	16431
Independent reflections	4777
$F_o > 4\sigma F$	3329
Refinement method	Full-matrix least squares on F^2, fixed weights proportional to $1/\sigma F_o^2$
No. of refined parameters	369
Final R_{obs} (%)	
$[F_o > 4\sigma F]$	9.09
R_1	12.02
wR_2	23.20
Highest peak, deepest hole (e Å^{-3})	1.90
	1.34
Goodness of fit on F^2	1.100

assign Si with minor Al to ten tetrahedral *Si* sites, with <Si−O> = 1.615 Å.

Consider next the octahedral sites in the O sheet. There are nine independent [6]-coordinated *M* sites [*M*(1−9)], with the size of a corresponding octahedron increasing from *M*(1) to *M*(9); the *M*(1−9) sites can accommodate up to 17 a.p.f.u. Site-scattering for the *M* sites varies from 20 to 26 electrons per site (e.p.s.), with the lowest values observed at the *M*(7−9) sites. Total refined scattering at the *M* sites is 413.5 e.p.f.u., which agrees well with the calculated site-scattering from the remaining Fe^{3+} plus (Fe^{2+} + Mn^{2+} + Ca + Zn + Mg), with a vacancy of 0.66 p.f.u. On the basis of observed bond distances and incident bond-valence at these sites (Table 8), we assign 2/3 of Fe^{3+} and 1/3 of Fe^{2+} to each *M*(1), *M*(2) and *M*(3) site (see above) (Table 7). We allocate the remaining Fe^{3+} equally to the *M*(4) and *M*(5) sites, plus an equal quantity of Mn^{2+} to account for the larger size of these two octahedra. The M(6) octahedron is larger and we assign the remaining Fe^{2+} and Mn^{2+} to the *M*(6) site. The larger *M*(7)−*M*(9) sites give different refined scattering values, being greater for the *M*(8) site, with the M(8) octahedron being slightly smaller than the M(7,9) octahedra. Therefore we assign all the Zn + Mg to the *M*(8) site, while Ca is distributed equally among the *M*(7) and *M*(9) sites, leaving a 15% vacancy at the latter two sites in agreement with the refined site-scattering at these sites (Table 7). Thus we have three Fe^{3+}-dominant *M*(1,2,3) sites [<M−φ> = 2.06 Å (where φ = O, OH)]; three Fe^{2+}-dominant *M*(4,5,6) sites [<M−φ> = 2.14 Å] and three Mn^{2+}-dominant *M*(7,8,9) sites [<M−φ> = 2.21 Å].

Consider the interstitial *A*(1,2) and *B* sites, with refined site-scattering values of 26.89, 17.53 and 11.32 e.p.f.u., respectively (Table 7). The cations to be assigned to these sites are Na, Ba, Sr, K and Cs, with a total scattering of 55.74 e.p.f.u. (Table 7). *A*(2) is split into four sites: *A*(2A), *A*(2B), *A*(2C) and *A*(2D). The A(1) and A(2A−2D) polyhedra are larger (mean bond distances of 3.17 and 3.26 Å, respectively),

TABLE 5. Final atom coordinates and displacement parameters (Å^2) for veblenite.

Atom	Site occ. (%)	*x*	*y*	*z*	U_{iso}*
Si(1)	100	0.9550(9)	0.3400(3)	0.2837(4)	0.0110(12)
Si(2)	100	0.4407(9)	0.2992(3)	0.3066(4)	0.0096(11)
Si(3)	100	0.3956(10)	0.2023(3)	0.3330(4)	0.0140(12)
Si(4)	100	0.8699(10)	0.1504(3)	0.3351(4)	0.0137(12)
Si(5)	100	0.1114(8)	0.6614(3)	0.1994(4)	0.0019(10)
Si(6)	100	0.2164(8)	0.8294(3)	0.2430(4)	0.0044(10)
Si(7)	100	0.2782(10)	0.9679(3)	0.3005(4)	0.0126(12)
Si(8)	100	0.1849(9)	0.9672(3)	0.6785(4)	0.0138(12)
Si(9)	100	0.9889(8)	0.5780(3)	0.7670(4)	0.0033(10)
Si(10)	100	0.9462(8)	0.4522(3)	0.8048(4)	0.0009(10)
D(1A)	50	0.6507(9)	0.7277(3)	0.1852(4)	0.0021(16)
D(1B)	50	0.6366(8)	0.7140(3)	0.1559(5)	0.0021(7)
D(2A)	50	0.4996(9)	0.5522(7)	0.8505(12)	0.0021(7)
D(2B)	50	0.4862(13)	0.5355(10)	0.8217(17)	0.0021(7)
M(1)	100	½	0	½	0.0058(9)
M(2)	100	0.6415(4)	0.27139(14)	0.5679(2)	0.0077(6)
M(3)	100	0.7330(4)	0.47901(15)	0.5129(2)	0.0082(7)
M(4)	100	0.8706(5)	0.78595(15)	0.4275(2)	0.0111(7)
M(5)	100	0.1885(5)	0.33821(15)	0.5775(2)	0.0136(7)
M(6)	100	0.9518(5)	0.92035(16)	0.4611(2)	0.0164(7)
M(7)	85	0.7035(6)	0.3899(2)	0.5641(3)	0.0114(8)
M(8)	97	0.2361(6)	0.4400(2)	0.5521(3)	0.0287(9)
M(9)	85	0.4225(7)	0.8513(2)	0.4410(3)	0.0179(9)
A(1)	83	½	½	0	0.0334(17)
A(2A)	10	0.645(12)	0.751(4)	0.007(4)	0.0334(17)
A(2B)	10	0.502(11)	0.751(3)	–0.003(4)	0.0334(17)
A(2C)	10	0.786(13)	0.759(3)	0.008(4)	0.0334(17)
A(2D)	10	0.640(8)	0.765(3)	0.999(4)	0.0334(17)
B	44	0.075(3)	0.6442(11)	0.0033(17)	0.0334(17)
O(1)	100	0.610(3)	0.1508(9)	0.2902(12)	0.034(4)
O(2)	100	0.106(3)	0.1559(9)	0.2914(12)	0.033(4)
O(3)	100	0.409(2)	0.2264(8)	0.2770(11)	0.023(3)
O(4)	100	0.169(3)	0.2921(8)	0.2517(12)	0.028(3)
O(5)	100	0.674(3)	0.2927(8)	0.2482(12)	0.028(3)
O(6)	100	0.336(2)	0.6686(8)	0.1557(11)	0.020(3)
O(7)	100	0.840(2)	0.6550(7)	0.1505(10)	0.016(3)
O(8)	100	0.947(3)	0.7701(8)	0.1776(11)	0.027(3)
O(9)	100	0.446(3)	0.7849(9)	0.1904(13)	0.037(4)
O(10)	100	0.224(2)	0.8787(7)	0.2257(10)	0.018(3)
O(11)	100	0.929(2)	0.2239(7)	0.4753(10)	0.013(3)
O(12)	100	0.463(2)	0.2767(7)	0.4721(10)	0.015(3)
O(13)	100	0.516(2)	0.3798(7)	0.4433(9)	0.009(3)
O(14)	100	0.019(2)	0.4234(6)	0.4200(9)	0.007(3)
O(15)	100	0.168(2)	0.7335(7)	0.3381(10)	0.012(3)
O(16)	100	0.262(2)	0.8908(7)	0.3812(10)	0.014(3)

Table 5 (*contd.*)

Atom	Site occ. (%)	*x*	*y*	*z*	U_{iso}*
O(17)	100	0.665(2)	0.9708(7)	0.5625(10)	0.009(3)
O(18)	100	0.117(2)	0.8979(7)	0.5387(9)	0.009(3)
O(19)	100	0.924(2)	0.4952(7)	0.6295(11)	0.019(3)
O(20)	100	0.886(2)	0.3794(7)	0.6669(10)	0.014(3)
O(21)	100	0.909(2)	0.4196(8)	0.8494(11)	0.022(3)
O(22)	100	0.755(2)	0.5068(7)	0.8520(11)	0.019(3)
O(23)	100	0.232(2)	0.4986(8)	0.8535(11)	0.021(3)
O(24)	100	0.751(2)	0.5900(8)	0.8223(11)	0.024(3)
O(25)	100	0.238(3)	0.5840(8)	0.8247(12)	0.030(4)
O(26)	100	0.045(2)	0.6490(7)	0.7894(10)	0.011(3)
O(27)	100	0.165(3)	0.9313(8)	0.7159(12)	0.031(4)
O(28)	100	0.474(3)	0.0178(10)	0.7312(14)	0.044(4)
O(29)	100	0.971(3)	0.0226(9)	0.7353(13)	0.035(4)
$X_D^O(1)$	100	0.726(2)	0.8043(8)	0.3449(11)	0.021(3)
$X_D^O(2)$	100	0.416(2)	0.4431(8)	0.6639(11)	0.023(3)
$X_A^O(1)$	100	0.003(2)	0.3369(7)	0.4758(10)	0.017(3)
$X_A^O(2)$	100	0.207(2)	0.0383(7)	0.5868(10)	0.016(3)
$X_A^O(3)$	100	0.591(2)	0.8311(7)	0.5224(10)	0.010(3)
$X_A^O(4)$	100	0.456(2)	0.5325(7)	0.5968(10)	0.013(3)
$X_A^O(5)$	100	0.357(2)	0.3192(7)	0.6549(11)	0.019(3)
X_D^P	100	0.5700(19)	0.6418(6)	0.0038(9)	0.004(2)
W(1)	57	0.814(6)	0.1264(18)	0.106(3)	0.05**
W(2)	43	0.745(8)	0.013(2)	0.885(3)	0.05**
W(3)	23	0.734(15)	0.160(4)	0.990(6)	0.05**
W(4)	17	0.623(18)	0.864(6)	0.997(8)	0.05**
W(5)	21	0.941(16)	0.160(5)	0.989(7)	0.05**
Subsidiary peaks					
M(1A)‡	5	0.521(9)	–0.008(3)	0.457(5)	0.01**
M(6A)	2	0.91(2)	0.875(8)	0.358(12)	0.01**
M(9A)	6	0.474(8)	0.917(3)	0.586(4)	0.01**

* U_{eq} for Si(1–8), M(2–9), A(1), A(2A–2D), B; ** fixed; ‡ scattering curves of Fe^{2+}, Fe^{2+} and Mn were used in the refinement of site occupancies of M(1A), M(6A) and M(9A), respectively.

while the B polyhedron is smaller, with <B–φ> = 2.72 Å, and the *B* site has lower scattering than the *A* sites. Therefore, we allocate all the available Na as well as the remaining Ca to the *B* site, which yields 11.32 e.p.f.u. in good agreement with the refined value of 11.3(4) e.p.f.u. Vacancy is therefore dominant at the *B* site (Table 7). The greater refined scattering at the *A*(1) site forces us to assign all the Ba + Sr from the analysis to that site. Cs is the largest cation left to be assigned and we consequently allocate it to the *A*(2A–2D) sites. The remaining K was distributed so that the best agreement with the refined site-scattering was obtained (Table 7). The *A*(1) site is K dominant, while the *A*(2A–2D) sites are vacancy dominant.

General topology of the crystal structure

The crystal structure of veblenite consists of HOH layers stacked along **c** (Fig. 3): two H sheets and an O sheet constitute an HOH layer,

TABLE 6. Selected interatomic distances (Å) and angles (°) in veblenite.

Si(1)–O(4)d	1.61(1)	Si(2)–O(3)	1.60(1)	Si(3)–O(3)	1.61(1)	Si(4)–O(1)	1.59(2)
Si(1)–O(26)c	1.61(1)	Si(2)–O(13)	1.61(1)	Si(3)–O(2)	1.62(1)	Si(4)–O(2)d	1.60(2)
Si(1)–O(5)	1.61(1)	Si(2)–O(5)	1.64(1)	Si(3)–O(12)	1.63(1)	Si(4)–O(27)c	1.61(2)
Si(1)–O(14)d	1.62(1)	Si(2)–O(4)	1.65(1)	Si(3)–O(1)	1.63(2)	Si(4)–O(11)	1.64(1)
<Si(1)–O>	1.61	<Si(2)–O>	1.63	<Si(3)–O>	1.62	<Si(4)–O>	1.61
Si(5)–O(6)	1.57(1)	Si(6)–O(8)a	1.59(1)	Si(7)–O(29)c	1.60(2)	Si(8)–O(27)	1.59(2)
Si(5)–O(7)a	1.60(1)	Si(6)–O(9)	1.60(2)	Si(7)–O(10)	1.61(1)	Si(8)–O(28)k	1.62(2)
Si(5)–O(21)c	1.62(1)	Si(6)–O(10)	1.62(1)	Si(7)–O(28)c	1.62(2)	Si(8)–O(18)	1.64(1)
Si(5)–O(15)	1.62(1)	Si(6)–O(16)	1.65(1)	Si(7)–O(17)f	1.63(1)	Si(8)–O(29)o	1.66(2)
<Si(5)–O>	1.60	<Si(6)–O>	1.62	<Si(7)–O>	1.62	<Si(8)–O>	1.63
Si(9)–O(24)	1.59(1)	Si(10)–O(22)	1.57(1)	Si(3)–O(1)-Si(4)	142.6(1.0)		
Si(9)–O(25)d	1.59(1)	Si(10)–O(23)d	1.58(1)	Si(3)–O(2)-Si(4)a	143.4(1.0)		
Si(9)–O(19)	1.63(1)	Si(10)–O(20)	1.61(1)	Si(2)–O(3)-Si(3)	143.3(9)		
Si(9)–O(26)d	1.64(1)	Si(10)–O(21)	1.63(1)	Si(1)a–O(4)-Si(2)	142.4(1.0)		
<Si(9)–O>	1.61	<Si(10)–O>	1.60	Si(1)–O(5)-Si(2)	140.3(1.0)		
				Si(6)–O(10)-Si(7)	139.9(8)		
				Si(5)–O(21)-Si(10)	139.1(1.9)		
				Si(1)–O(26)-Si(9)	138.8(8)		
				Si(4)c–O(27)-Si(8)	142.0(1.0)		
				Si(7)c–O(28)-Si(8)f	143.4(1.1)		
				Si(7)c–O(29)-Si(8)g	141.1(1.0)		
D(1A)-X_D^O(1)	1.88(1)	D(1B)–X_D^P	1.79(1)	D(2A)–X_D^Pb	1.81(2)	D(2B)–X_D^O(2)	1.86(2)
D(1A)–O(6)	1.95(1)	D(1B)–O(6)	1.94(1)	D(2A)–O(25)	1.95(1)	D(2B)–O(25)	1.95(2)
D(1A)–O(9)	1.95(2)	D(1B)–O(8)	1.95(1)	D(2A)–O(24)	1.96(1)	D(2B)–O(24)	1.96(1)
D(1A)–O(8)	1.96(1)	D(1B)–O(9)	1.95(2)	D(2A)–O(22)	1.96(1)	D(2B)–O(22)	1.96(1)
D(1A)–O(7)	1.98(1)	D(1B)–O(7)	1.99(1)	D(2A)–O(23)	1.99(1)	D(2B)–O(23)	2.00(1)
D(1A)–X_D^P	2.14(1)	D(1B)–X_D^O(1)	2.23(1)	D(2A)–X_D^O(2)	2.20(2)	D(2B)–X_D^Pb	2.15(2)
<D(1A)–O>	1.98	<D(1B)–O>	1.98	<D(2A)–O>	1.98	<D(2B)–O>	1.98
M(1)–X_A^O(2)	2.05(1) x2	M(2)–X_A^O(5)	2.02(1)	M(3)–X_A^O(4)	1.99(1)	M(4)–X_A^O(3)	2.05(1)
M(1)–O(16)e	2.07(1) x2	M(2)–X_A^O(3)c	2.03(1)	M(3)–X_A^O(4)c	2.01(1)	M(4)–X_D^O(1)	2.10(1)
M(1)–O(17)c	2.07(1) x2	M(2)–O(11)	2.07(1)	M(3)–O(19)	2.05(1)	M(4)–O(15)d	2.11(1)
<M(1)–O>	2.06	M(2)–O(15)c	2.09(1)	M(3)–O(13)	2.06(1)	M(4)–X_A^O(5)c	2.12(1)
		M(2)–O(12)	2.10(1)	M(3)–O(14)d	2.09(1)	M(4)–O(18)d	2.15(1)
		M(2)–O(20)	2.12(1)	M(3)–O(14)c	2.12(1)	M(4)–O(11)j	2.27(1)
		<M(2)–O>	2.07	<M(3)–O>	2.05	<M(4)–O>	2.13

M(5)–X^{O}_{A}(1)	2.07(1)	M(6)–O(16)d	2.08(1)	M(7)–X^{O}_{A}(1)d	2.12(1)	M(8)–X^{O}_{A}(1)	2.13(1)
M(5)–X^{O}_{A}(5)	2.08(1)	M(6)–X^{O}_{A}(2)c	2.12(1)	M(7)–X^{O}_{D}(2)	2.14(1)	M(8)–X^{O}_{A}(4)	2.14(1)
M(5)–X^{O}_{D}(2)	2.09(1)	M(6)–O(17)	2.14(1)	M(7)–O(13)	2.22(1)	M(8)–O(19)a	2.14(1)
M(5)–O(20)a	2.11(1)	M(6)–O(18)d	2.15(1)	M(7)–O(19)	2.24(1)	M(8)–O(13)	2.19(1)
M(5)–O(12)	2.14(1)	M(6)–X^{O}_{D}(1)	2.16(1)	M(7)–O(12)	2.25(1)	M(8)–X^{O}_{D}(2)	2.19(1)
M(5)–O(11)a	2.26(1)	M(6)–X^{O}_{A}(2)p	2.23(1)	M(7)–O(20)	2.33(1)	M(8)–O(14)	2.35(1)
<M(5)–O>	2.13	<M(6)–O>	2.15	<M(7)–O>	2.22	<M(8)–O>	2.19
M(9)–X^{O}_{A}(3)	2.17(1)	A(1)–O(7)	2.98(1) x2	A(2A)–X^{P}_{D}	2.94(9)	A(2B)-W(3)c	2.71(9)
M(9)–X^{O}_{D}(1)	2.17(1)	A(1)–O(23)i	3.00(1) x2	A(2A)–O(24)i	3.00(7)	A(2B)–O(25)i	3.00(5)
M(9)–O(18)	2.19(1)	A(1)–O(21)i	3.11(1) x2	A(2A)–O(9)j	3.07(8)	A(2B)–O(9)	3.01(5)
M(9)–O(17)	2.24(1)	A(1)–O(22)i	3.27(1) x2	A(2A)-W(5)	3.09(12)	A(2B)-W(4)i	3.12(11)
M(9)–O(16)	2.26(1)	A(1)–O(21)h	3.32(1) x2	A(2A)–O(8)	3.13(8)	A(2B)–O(26)i	3.14(5)
M(9)–O(15)	2.31(1)	A(1)–O(6)	3.32(1) x2	A(2A)–O(25)i	3.26(7)	A(2B)–X^{P}_{D}	3.17(5)
<M(9)–O>	2.22	<A(1)–O>	3.17	A(2A)-W(4)i	3.29(14)	A(2B)–O(10)	3.39(5)
				A(2A)-W(3)c	3.30(12)	A(2B)–O(24)i	3.39(5)
				A(2A)–O(10)d	3.63(6)	A(2B)-W(5)c	3.44(10)
				<A(2A)–O>	3.19	A(2B)-W(5)j	3.50(10)
						<A(2B)–O>	3.19
						B–O(8)a	2.54(2)
A(2C)-W(5)j	2.51(10)	A(2D)-W(5)n	2.76(11)	Short distances		B–O(25)i	2.60(2)
A(2C)–O(24)i	2.93(6)	A(2D)-W(4)	2.77(13)			B–O(6)	2.64(2)
A(2C)–O(8)	3.01(5)	A(2D)-W(3)m	2.91(10)	D(1A)-D(1B)	0.345(6)	B–O(22)h	2.65(2)
A(2C)–O(10)d	3.13(6)	A(2D)–O(24)	3.29(6)	D(2A)-D(2B)	0.338(8)	B–X^{P}_{D}	2.67(2)
A(2C)–O(26)l	3.19(6)	A(2D)–O(9)b	3.43(7)	A(2A)-A(2B)	0.78(6)	B–X^{P}_{D}a	2.71(2)
A(2C)-W(3)j	3.22(10)	A(2D)–X^{P}_{D}b	3.46(8)	A(2A)-A(2C)	0.76(6)	B–O(24)h	2.80(2)
A(2C)–X^{P}_{D}	3.25(6)	A(2D)–O(25)	3.51(6)	A(2B)-A(2C)	1.50(7)	B–O(9)	2.85(2)
A(2C)-W(4)i	3.27(11)	A(2D)–O(8)b	3.55(7)	A(2B)-A(2D)i	0.79(6)	B–O(23)i	2.87(2)
A(2C)–O(9)	3.55(6)	A(2D)–O(26)	3.63(4)	A(2C)-A(2D)i	0.86(7)	B–O(7)	2.91(2)
<A(2C)–O>	3.12	<A(2D)–O>	3.26			<B–O>	2.72

Symmetry operators: a: $x-1, y, z$; b: $x, y, z+1$; c: $-x+1, -y+1, -z+1$; d: $x+1, y, z$; e: $x, y-1, z$; f: $-x+1, -y+2, -z+1$; g: $x+1, y-1, z$; h: $x-1, y, z-1$; i: $x, y, z-1$; j: $-x+2, -y+1, -z+1$; k: $x, y+1, z$; l: $x+1, y, z-1$; m: $-x+1, -y+1, -z+2$; n: $-x+2, -y+1, -z+2$; o: $x-1, y+1, z$; p: $x+1, y+1, z$.

TABLE 7. Refined site-scattering (e.p.f.u.) and assigned site-populations (a.p.f.u.) for veblenite*.

Site**	Refined site-scattering	Site population	Calculated site-scattering	<X−φ>$_{calc.}$ (Å)	<X−φ>$_{obs.}$ (Å)
D(1A)	35.02(6)	0.55 Nb + 0.28 Ti + 0.17 Fe^{3+} + 1.00 □	33.10	2.01	1.98
D(1B)	41.1(6)	0.90 Nb + 0.10 Ti + 1.00 □	37.20	2.02	1.98
D(2A)	45.8(3.0)	11.00 Nb + 1.00 □	41.00	2.02	1.98
D(2B)	31.5(3.0)	0.55 Ti + 0.45 Nb + 1.00 □	30.60	2.00	1.98
Total *D*	153.42	2.90 Nb + 0.93 Ti + 0.17 Fe^{3+}	141.19		
M(1)	26.0	0.67 Fe^{3+} + 0.33 Fe^{2+}	26.00	2.06	2.06
M(2)	52.0	1.34 Fe^{3+} + 0.66 Fe^{2+}	52.00	2.06	2.07
M(3)	52.0	1.34 Fe^{3+} + 0.66 Fe^{2+}	52.00	2.06	2.05
M(4)	52.0	1.22 Fe^{2+} + 0.39 Fe^{3+} + 0.39 Mn	51.61	2.13	2.13
M(5)	52.0	1.22 Fe^{2+} + 0.39 Fe^{3+} + 0.39 Mn	51.61	2.13	2.13
M(6)	52.0	1.23 Fe^{2+} + 0.77 Mn	51.23	2.17	2.15
M(7)	40.0	1.35 Mn + 0.35 Ca + 0.30 □	40.75	2.24	2.22
M(8)	47.5	1.72 Mn + 0.15 Zn + 0.07 Mg + 0.06 □	48.34	2.19	2.19
M(9)	40.0	1.35 Mn + 0.35 Ca + 0.30 □	40.75	2.24	2.22
Total *M*	413.5	5.32 Fe^{2+} + 4.13 Fe^{3+} + 5.97 Mn + 0.70 Ca + 0.15 Zn + 0.07 Mg + 0.66 □	414.29		
$^{[12]}A$(1)	26.6(5)	0.53 K + 0.28 Ba + 0.03 Sr + 0.16 □	26.89		3.17
$^{[9]}A$(2A)	5.2(1.3)				3.19
$^{[10]}A$(2B)	4.5(5)				3.19
$^{[9]}A$(2C)	3.8(5)				3.12
$^{[9]}A$(2D)	5.7(1.3)				3.12
Total *A*(2)	19.2	1.21 □ + 0.72 K + 0.07 Cs	17.53		3.26
$^{[10]}B$	11.3(4)	1.11 □ + 0.72 Na + 0.17 Ca	11.32		2.72

* X = cation; φ = unspecified anion, φ = O, OH, F, H_2O; <X-φ> calculated using ionic radii of Shannon (1976); ** coordination number is shown in brackets for non-octahedral sites.

Table 8. Bond-valence values* for veblenite.

Atom	Si(1)	Si(2)	Si(3)	Si(4)	Si(5)	Si(6)	Si(7)	Si(8)	Si(9)	Si(10)	D(1A)	D(1B)	D(2A)	D(2B)	M(1)	M(2)	M(3)	M(4)	M(5)	M(6)	M(7)	M(8)	M(9)	A(1)	B	Σ
$^{[2]}$O(1)			0.98	1.09																						2.07
$^{[2]}$O(2)			1.01	1.06																						2.07
$^{[2]}$O(3)		1.06	1.03																							2.09
$^{[2]}$O(4)	1.03	0.93																								1.96
$^{[2]}$O(5)	1.03	0.95																								1.98
O(6)					1.15						0.39	0.45												0.04$^{x2}\downarrow$	0.06	2.09
O(7)					1.06						0.36	0.39												0.10$^{x2}\downarrow$	0.04	1.95
O(8)						1.09					0.38	0.44													0.08	1.99
O(9)						1.06					0.39	0.44													0.05	1.94
$^{[2]}$O(10)						1.01	1.03																			2.04
O(11)				0.95												0.42		0.25	0.26							1.88
O(12)			0.98													0.39			0.35		0.26					1.98
O(13)		1.03															0.43				0.28	0.31				2.05
O(14)	1.01																0.40					0.21				1.99
																	0.37									
O(15)					1.01											0.40		0.38					0.23			2.02
O(16)						0.93									0.42$^{x2}\downarrow$					0.42			0.26			2.03
O(17)							0.98								0.42$^{x2}\downarrow$					0.36			0.27			2.03
O(18)								0.95										0.33		0.35			0.31			1.94
O(19)									0.98								0.44				0.27	0.35				2.04
O(20)										1.03						0.37			0.38		0.22					2.00
O(21)					1.01					0.98														0.07$^{x2}\downarrow$		2.10
																								0.04$^{x2}\downarrow$		
O(22)										1.15			0.44	0.38										0.05$^{x2}\downarrow$	0.06	2.08
O(23)										1.12			0.40	0.34										0.09$^{x2}\downarrow$	0.04	1.99
O(24)									1.09				0.44	0.38											0.05	1.96
O(25)									1.09				0.45	0.39											0.07	2.00
$^{[2]}$O(26)	1.03								0.95																	1.98
$^{[2]}$O(27)				1.03				1.09																		2.12
$^{[2]}$O(28)							1.01	1.01																		2.02
O(29)							1.06	0.91																		1.97
X^{O}_{D}(1)											0.47	0.22						0.39		0.34			0.32			1.74
X^{O}_{D}(2)													0.24	0.49					0.40		0.35	0.31				1.71
$^{[3]}X^{O}_{A}$(1)																			0.42		0.37	0.36				1.15
$^{[3]}X^{O}_{A}$(2)															0.44$^{x2}\downarrow$					0.38						1.10
																				0.28						
$^{[3]}X^{O}_{A}$(3)																0.47		0.45					0.32			1.24
$^{[3]}X^{O}_{A}$(4)																	0.53					0.35				1.38
																	0.50									
$^{[3]}X^{O}_{A}$(5)																0.48		0.37	0.41							1.26
X^{P}_{D}											0.24	0.67	0.65	0.24											0.06	1.92
																									0.06	
Total	4.10	3.97	4.00	4.13	4.23	4.09	4.08	3.96	4.11	4.28	2.23	2.61	2.62	2.22	2.56	2.53	2.67	2.17	2.22	2.13	1.75	1.88	1.71	0.78	0.57	
Aggr. charge	4.00	4.00	4.00	4.00	4.00	4.00	4.00	4.00	4.00	4.00	2.19	2.45	2.50	2.23	2.67	2.67	2.67	2.20	2.20	2.00	1.70	1.94	1.70	1.15	0.53	

* Bond-valence parameters are from Brown (1981); coordination numbers are shown for non [4]-coordinated anion; bond-valence values are not calculated from K atoms at the A(2A-2D) sites (~10% occupancy); X^{O}_{A}(1-5) are either O atoms of OH groups or F atoms.

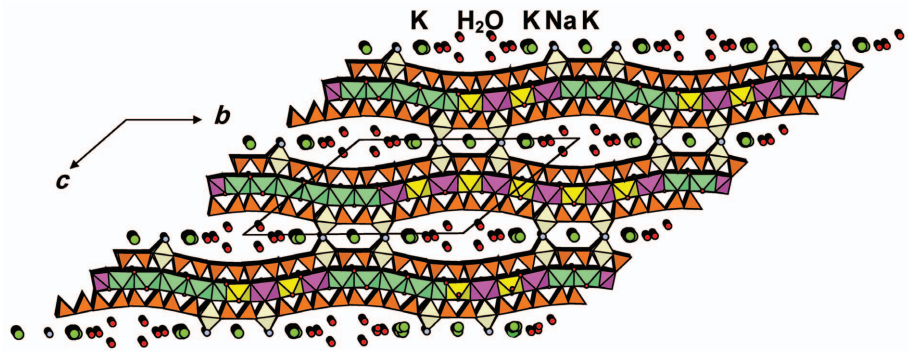

FIG. 3. General view of the crystal structure of veblenite. Si tetrahedra are orange, Fe^{2+}-, Fe^{3+}- and Mn-dominant M octahedra are green, yellow and pink, (Nb,Ti) D octahedra are pale yellow; K- and Na- dominant *A*(1), *A*(2) and *B* sites are shown as green and blue spheres, respectively; OH and H_2O groups are shown as small and large red spheres. The unit cell is shown with thin black lines.

with a new topology that has not been found in any other HOH structures. M octahedra share common edges to form a modulated trioctahedral close-packed (O) sheet parallel to (001) (Fig. 3). The H sheet is composed of Si_2O_7 groups, Si_8O_{22} ribbons and [6]-coordinated Nb-dominant D octahedra (Fig. 4*b*). Two H sheets of the HOH layer are identical. This is the first occurrence of a Si_8O_{22} ribbon in a mineral structure, and we call it the *veblenite* ribbon. This is also the first occurrence of the H sheets of the composition $[Nb_3Ti(Si_2O_7)_2(Si_8O_{22})_2]^{15-}$. H sheets link to the central O sheet *via* common anions of M octahedra and Si and D polyhedra. The t_1 repeat of ~5.5 Å is common to Ti-disilicates (Sokolova, 2006) and astrophyllite-group minerals (Sokolova, 2012). The HOH layers are stacked along [001] and show a lateral shift along [010], which allows linkage *via* common anions of D polyhedra of the H sheets. This type of linkage yields two types of channels running along [100]: wide and narrow channels that alternate in both [010] and [001] directions (Fig. 5*a*). Along [100], interstitial *B* sites are partly occupied by Na (Fig. 5*a*). Within the narrow [100] channels, *A*(1) interstitial sites are almost fully occupied by K (Fig. 5*a*), while at the narrower sides of the wide [001] channels, there are interstitial K cations in partially occupied A(2A–D) split positions. In the central part of the wide channels, H_2O groups coordinate K at the *A*(2) sites (Fig. 5*a*).

The crystal structure of veblenite is closely related to the structure of nafertisite, ideally $(Na,K)_2(Fe^{2+},Fe^{3+},\square)_{10}[Ti_2(Si,Fe^{3+},Al)_{12}O_{37}](OH,O)_6$ (Ferraris *et al*., 1996), niobophyllite, ideally $K_2NaFe^{2+}_7(Nb,Ti)_2(Si_4O_{12})_2O_2(OH)_4(O,OH)$ (Cámara *et al*., 2010), an astrophyllite-group mineral, and jinshaijangite, ideally $NaBaFe^{2+}_4Ti_2(Si_2O_7)_2O_2(OH)_2F$ (Sokolova *et al*., 2009), a TS-block mineral of Group II (Sokolova, 2006). The topology of the veblenite structure was generated by Hawthorne (2012) who used a structure-generating function for polysomatic TOT and HOH structures.

Description of cation and anion sites

Cation sites

The crystal structure contains three groups of cation sites: *D* and *Si* sites of the H sheet, *M* sites of the O sheet, and interstitial *A* and *B* sites (see above).

O sheet

There are nine cation sites in the O sheet: the Fe^{3+}-dominant *M*(1,2,3) sites, the Fe^{2+}-dominant *M*(4,5,6) sites and Mn^{2+}-dominant *M*(7,8,9) sites (Fig. 4*a*). Fe^{3+} occurs only at the *M*(1–6) sites and vacancies are present at the *M*(7,8,9) sites. The *M*(1,2,3) sites are occupied by 2/3 Fe^{3+} and 1/3 Fe^{2+} with <M(1,2,3)–φ> = 2.06 Å (φ = unspecified anion), and are coordinated by four O atoms shared with Si atoms and two monovalent X^O_A anions (see section on *Anion sites* below) (Tables 6 and 7). The *M*(4,5) sites are occupied by 0.62 Fe^{2+} a.p.s., 0.19 a.p.s. Fe^{3+} and 0.19 Mn^{2+} a.p.f. with <M(4,5)-φ> = 2.13 Å, and are coordinated by three O atoms shared with Si atoms, one O atom at the X^O_D site (shared with a *D*

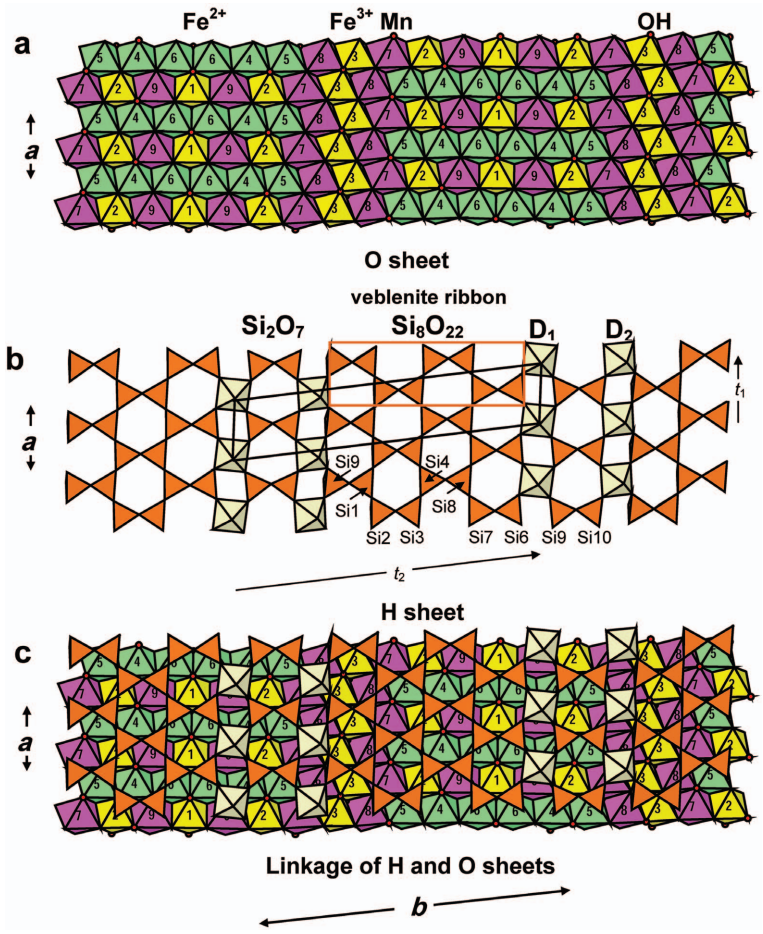

FIG. 4. The HOH layer in veblenite: (*a*) the O sheet; (*b*) the H sheet in veblenite shows two types of Si-O radicals: Si_2O_7 groups and a new veblenite Si_8O_{22} ribbon; the repeat of the veblenite ribbon is indicated with a red box; (*c*) linkage of H and O sheets. Legend as in Fig. 3, Si tetrahedra are orange, (Nb,Ti) D octahedra are pale yellow. The unit cell is shown with thin black lines; in (a and c), M octahedra are numbered.

atom), and two monovalent X_A^O anions (Tables 6, 7 and 8). The *M*(6) site is occupied only by divalent cations (0.61 a.p.s. Fe^{2+} and 0.19 a.p.f. Mn^{2+}) with a <M(6)−φ> distance of 2.15 Å and, like the *M*(4,5) sites, it is coordinated by three O atoms shared with Si atoms, one X_D^O divalent anion occupied by oxygen, and two monovalent X_A^O anions (Tables 6, 7 and 8). The *M*(7,9) sites are occupied by 0.67 a.p.s. Mn^{2+}, 0.18 a.p.s. Ca and 0.15 vacancy and are coordinated by four O atoms shared with Si atoms, one X_D^O divalent anion occupied by oxygen, and one monovalent X_A^O anion, with a <M(7,9)−φ> distance of 2.22 Å, while the *M*(8) site is occupied by 0.86 a.p.s. Mn^{2+}, 0.08 a.p.s. Zn and 0.03 a.p.s. Mg and 0.03 vacancy per site and is coordinated by three O atoms shared with Si atoms, one X_D^O divalent anion occupied by oxygen, and two monovalent X_A^O anions, with <M(8)−φ> = 2.19 Å (Tables 6, 7 and 8). Cations of the O sheet sum to $(Fe^{2+}_{5.32}Fe^{3+}_{4.13}Mn^{2+}_{5.97}Ca_{0.70}Zn_{0.15}Mg_{0.07}\square_{0.66})$ a.p.f.u. (Table 7), with ideal and simplified compositions of $(Fe^{2+}_5Fe^{3+}_4Mn^{2+}_7\square)$ and $(Fe^{2+},Fe^{3+},Mn^{2+})_{17}$ a.p.f.u., respectively.

H sheets

In the H sheets, there are ten tetrahedrally coordinated sites occupied by Si with a <Si−O>

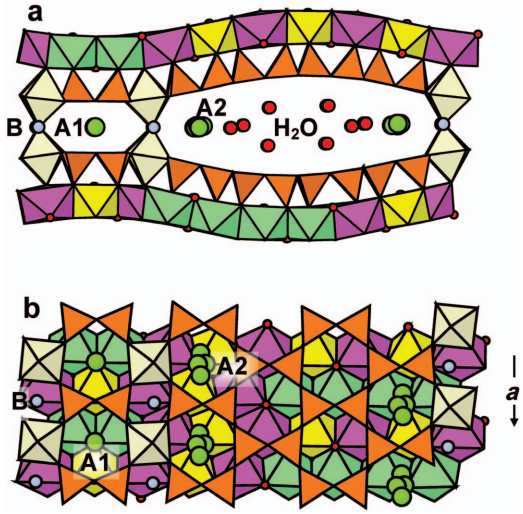

FIG. 5. General view of the narrow and wide [100]-channels in the structure of veblenite, showing the position of *A* and *B* sites and OH and H_2O groups: (*a*) projection along [100]; (*b*) projection along [001] (legend as in Fig. 3).

distance of 1.615 Å (Table 6, Fig. 4*b*,*c*). The longest Si−O distance is usually the one to the O atom shared with the M atoms in the O sheet. There are two Si tetrahedra that are slightly larger [Si(2) and Si(8), with <Si−O> = 1.63 Å] and the Si(2,8) sites may therefore host up to 10% Al. Interestingly, the Si(2,8) tetrahedra share an oxygen atom with two Mn^{2+}-dominant M(7,8) octahedra; i.e. two of the largest ones] and an Fe^{3+}-dominant M(3) octahedron], while all other Si tetrahedra share an apex with one Fe^{2+}-dominant, one Mn^{2+}-dominant and one Fe^{3+}-dominant octahedra, and would nominally have less incident bond valence. In fact, these two tetrahedral sites have the lowest incident bond-valence sums among all the *Si* sites (Table 8). Sokolova (2012) showed that Si_2O_7 groups of the astrophyllite Si_4O_{12} ribbon have a very restricted range of Si−O−Si angles, namely 138−143º, compared to the Si_2O_7 groups in the Ti-silicate minerals, which show a wider range of Si−O−Si angles: ~134 to ~206º (Sokolova, 2006). The Si−O−Si angles in veblenite range from 138 to 143º (Table 6) as in the astrophyllite-group structures, indicating reduced flexibility of the tetrahedral ribbons to match connectivity with the O sheet.

There are two [6]-coordinated *D*(1,2) sites that each split into two sites: *D*(1A, 1B) and *D*(2A, 2B). Each of the latter four sites is octahedrally coordinated by six O atoms, with <D−O> = 1.98 Å (Table 6). There are three Nb-dominant sites: *D*(1A,1B, 2A) and one Ti-dominant *D*(2B) site, with total $Nb_{2.90}Ti_{0.93}Fe^{3+}_{0.17}$, ideally Nb_3Ti a.p.f.u. (Table 7). In veblenite, D octahedra of adjacent HOH layers connect *via* a bridge oxygen at the X^P_D site (Fig. 3). Four of six O atoms coordinating each D atom are common to a D octahedron and four Si tetrahedra; one atom is common to a D octahedron and three M octahedra of the O sheet. The $X^O_D(1)$ atom belongs to the D(1A,1B) octahedra and the $X^O_D(2)$ atom belongs to the D(2A,2B) octahedra, and the sixth O atom occurs at the X^P_D site. The shortest and the longest $D-X^O_M$ distances are 1.86 Å and 2.23 Å, respectively, while the shortest and the longest $D-X^P_D$ distances are 1.79 Å and 2.15 Å, respectively (Fig. 6). These distances are within the observed distances for Nb and Ti at the M^H sites in the H sheet in Ti-disilicates: e.g. epistolite (Sokolova and Hawthorne, 2004), vuonnemite (Ercit *et al.*, 1998), bornemanite (Cámara and Sokolova, 2007), nechelyustovite (Cámara and Sokolova, 2009) and kazanskyite (Cámara *et al.*, 2012).

However we are left with a question: which two of four D(1A−2B) sites can form the $D-X^P_D-D$ bridges? To answer this, we must consider SRO (short-range order) arrangements.

Short-range order arrangements at the D sites. The X^P_D atom receives bond-valence contributions from atoms at four *D* and two *B* sites occupied at 50% mainly by Nb and Na (contributions from the *A*(2) site occupied by K at ~40% are too small and not considered here) (Table 7). Note that D(1A)−D(1B) and D(2A)−D(2B) occur at short distances of ~0.33 Å and cannot be occupied locally. Hence, in the structure, the X^P_D site is [4] coordinated by two *D* sites and two *B* sites. The incident bond-valence of 1.92 vu (valence units) at the X^P_D atom (Table 8) tell us that the X^P_D site is occupied by an O atom both in the long-range structure and short-range-order arrangements. Consider the short-range-ordered arrangement where all cation sites (*D* and *B*) are fully occupied, i.e. at 100%. To calculate the bond-valence contributions to the X^P_D atom from D and B atoms, we must multiply their bond-valence contributions by 2 (corresponding to 50% occupancy): 0.24 × 2 = 0.48 vu [D(1A)], 1.34 vu [D(1B)], 1.30 vu [D(2A)], 0.48 vu [D(2B)] and 0.24 vu (B × 2). Contributions from D(1A), D(2B) and 2 B atoms sum to 1.20 vu which is too low for

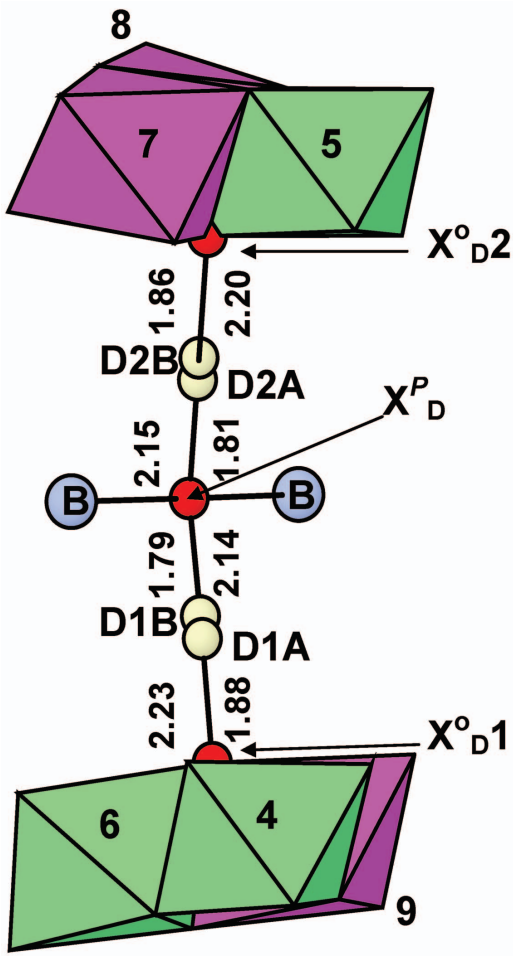

FIG. 6. Fragment of the crystal structure showing details of the linkage of two HOH layers via the bridge $D-X^{P}_{D}-D$. Nb and Na atoms at the *D* and *B* sites are shown as yellow and blue spheres, O atoms at the X^{P}_{D} and X^{O}_{D} sites are shown as red spheres, bonds between Nb and Na atoms and O atoms are shown as solid black lines; Fe^{2+}- and Mn-dominant octahedra in the O sheet are green and magenta and represent O sheets of different HOH layers.

an O atom. Contributions from the D(1B), D(2A) and 2B atoms sum to 2.88 vu which is too high for an O atom. We are left with two possible short-range-ordered arrangements: contributions from (1) [D(1A), D(2A) and 2B] and (2) [D(1B), D(2B) and 2B] atoms sum to 2.02 and 2.06 vu, respectively, compensating the 2^{-} charge of an O atom at the X^{P}_{D} site. Hence two types of $D-X^{P}_{D}-D$ bridges can occur in the structure: (SRO-1) D(1A)–O–D(2A) and (SRO-2) D(1B)–O–D(2B) (Fig. 6). The possible occurrence of these two short-range-ordered arrangements explains the difference in $D-X^{P}_{D}$ and $D-X^{O}_{D}$ distances. For SRO-1, D(1A)–O–D(2A), the X^{P}_{D} anion receives a larger bond-valence contribution from D(2A) (1.30 vu, shorter distance of 1.81 Å) and needs a smaller contribution from D(1A) (0.4 vu, longer distance of 2.14 Å). Note that the longer $D(1A)-X^{P}_{D}$ distance of 2.14 Å corresponds to the shorter $D(1A)-X^{O}_{D}(1)$ distance of 1.88 Å [cf. $D(2A)-X^{P}_{D}$ = 1.81 Å *vs.* $D(2A)-X^{O}_{D}(2)$ = 2.20 Å] (Fig. 6). It seems that the order of M cations in the O sheet forces the D atoms to change their positions in order to satisfy the bond-valence requirements at the X^{O}_{D} anions.

The D cations of two H sheets sum to $Nb_{2.90}Ti_{0.93}Fe^{3+}_{0.17}$ a.p.f.u. (Table 7), with ideal and simplified compositions of Nb_3Ti and $(Nb,Ti)_4$ a.p.f.u., respectively. We will consider the Si atoms as part of the complex oxyanions (see below).

Interstitial sites

In veblenite, there are two interstitial sites: *A* and *B*. There are two *A* sites: *A*(1) in the narrow channel and *A*(2) in the wider channel (Fig. 5*a*). The *A*(1) site is [12]-coordinated by the basal oxygen atoms of Si tetrahedra on both sides of the channel. It is almost fully occupied by 0.53 a.p.s. K, 0.28 a.p.s. Ba and 0.03 a.p.s. Sr and with 0.16 □ per site, and <A(1)–φ> = 3.17 Å (Table 6). We write the ideal and simplified compositions of the *A*(1) site as K and (K,Ba), respectively. The *A*(2) site is split in 4 mutually exclusive positions with partial occupancy (Table 7), being dominantly vacant (Fig. 5*b*). These split positions are [9–10]-coordinated by oxygen from the basal planes of tetrahedra of the adjacent H layers and by H_2O groups at partly occupied *W* sites (see section on *Anion sites* below), with <A(2A,2B)–φ> = 3.19 Å, <A(2C)–φ > = 3.12 Å, and <A(2D)–φ > = 3.26 Å. Aggregate composition for the *A*(2A–2D) sites is 0.60 □ p.s. + 0.36 a.p.s. K, and 0.04 a.p.s. Cs. We write the ideal and simplified compositions of the *A*(2) site as (□K) and $(□,K)_2$, respectively. The occupancy of *A*(2) sites is probably related to the $Nb_{-1}Ti$ substitution at the adjacent D sites. Therefore, the A(2) composition is constrained by the relation $A(2)_n = Nb_{4-n}Ti_n$, although the $Nb_{-1}Ti$ substitution could be compensated also by increasing the amount of

Fe^{3+} at the $M(1-3)$ sites.

The *B* site occurs between four *D* sites (from adjacent HOH layers, Fig. 5*a, b*); they are [10]-coordinated by the basal oxygen atoms of the Si tetrahedra of the adjacent HOH layers and by the oxygen atom shared by two D atoms from different HOH layers, with <B–O> = 2.72 Å. The *B* site is occupied at 45% by 0.36 a.p.s. Na and 0.09 a.p.s. Ca (Table 7). We write the ideal and simplified compositions of the *B* site as (□Na) and (□,Na), respectively, and the ideal and simplified compositions of the interstitial *A*(1)*A*(2)*B* sites are K(□K)(□Na) = $K_2\square_2Na$ and (K,Ba)(□,K)$_2$(□,Na)$_2$, respectively.

We write the cation part of the ideal and simplified formulae as the sum of the *M* sites of the O sheet + *D* sites of two H sheets + interstitial *A* and *B* sites: (1) ideal formula: $(Fe_5^{2+}Fe_4^{3+}Mn_7^{2+}\square)$ + Nb_3Ti + K(□K)(□Na) = $K_2\square_2Na(Fe_5^{2+}Fe_4^{3+}Mn_7^{2+}\square)Nb_3Ti$, with a total charge of 58^+; (2) simplified formula: $(Fe^{2+},Fe^{3+},Mn^{2+})_{17}$ + $(Nb,Ti)_4$ + (K,Ba)(□,K)$_2$(□,Na)$_2$ = [(K,Ba,□)$_3$(□,Na)$_2$ $(Fe^{2+},Fe^{3+},Mn^{2+})_{17}(Nb,Ti)_4$] a.p.f.u.

Anion sites

Following the nomenclature of the anion sites by Sokolova (2012), we label the X anions: 2 X_D^O = anions at common vertices of 3 M and D polyhedra; 5 X_A^O = monovalent anions at common vertices of 3 M polyhedra; X_D^P = apical anion shared by two D cations from two different HOH layers. Additionally, there are 5 interstitial H_2O groups (with partial occupancy) which we label W(1–5).

There are 29 anion sites, O(1–29), occupied by O atoms which form the tetrahedral coordination of the Si atoms (Tables 5, 6). Si(1–8) and O(1–29) atoms form two distinct complex oxyanions, $(Si_2O_7)_2$ and $(Si_8O_{22})_2$ p.f.u. There are two sites, $X_D^O(1,2)$, which are common anions for the D polyhedra and three octahedra of the O sheet (Tables 5, 6) and give O_4 p.f.u. These anions receive bond valences of 1.71–1.74 vu (Table 8) and hence are O atoms. The low incident bond-valence is probably due to the split of the *D* sites. There is one anion, X_D^P, shared by two *D* atoms of adjacent HOH layers; this anion receives a bond valence of 1.92 vu (Table 8) and hence is an O atom. The X_D^P site gives O_2 p.f.u. There are five $X_A^O(1-5)$ sites that are common anions for three octahedra of the O sheet. They receive bond valences of 1.20–1.38 vu (Table 8), and hence are monovalent anions (OH or F). The chemical analysis gives F 0.38 a.p.f.u. and we need 10 – 0.38 = 9.62 OH p.f.u. to fill these five sites. Therefore, we assign $OH_{9.62}F_{0.38}$ to the five $X_A^O(1-5)$ sites. Ideally, the five X_A^O sites give $(OH)_{10}$ p.f.u. There are H_2O groups at the five *W*(1–5) sites, and the O atoms of the H_2O groups are bonded to the A(2A–2D) cations. The *W*(1–5) sites are partly occupied (Table 5): *W*(1) and *W*(2) at 57 and 43%, and *W*(3,4,5) at 23, 17 and 21%, respectively. Local occupancy of both *W*(1) and *W*(2) is incompatible as W(1)–W(2) = 2.59(5) Å. Each H_2O group at one of these two sites bonds weakly to the basal oxygen atoms of the tetrahedra in the Si_8O_{22} ribbon. Occupancy of the *W*(3) site cannot be locally associated with occupancy of the *W*(4) and *W*(5) sites as W(3)–W(5) = 1.11(12) Å and W(3)–W(5) = 2.06(15) Å. The occupancy of the *W*(3–5) sites is linked to the occupancy of the *A*(2A–2D) sites. The observed occupancy of the *W*(3–5) sites is lower than that at the *A*(2A–2D) sites, probably due to the difficulty in correctly calculating the scattering at split positions with data from such a thin crystal. In veblenite, the *W*(1,2) and *W*(3–5) sites give $(H_2O)_2$ and $[(H_2O)_{1.23}\square_{2.77}]$ p.f.u., respectively, ideally $(H_2O)_3$ p.f.u.

To conclude, we write the anion part of the ideal structural formula as the sum of the complex anions and the simple anions (charge is given in brackets): $(Si_2O_7)_2$ (12^-) + $(Si_8O_{22})_2$ (24^-) + O_4 $[X_D^O(1,2)]$ (8^-) + O_2 $[X^P{}_D]$ (4^-) + $(OH)_{10}$ $[X_A^O(1-5)]$ (10^-) + $(H_2O)_3$ [W(1–5)] = $(Si_2O_7)_2(Si_8O_{22})_2$ $O_6(OH)_{10}(H_2O)_3$, with a total charge of 58^-.

Based on the SREF results and bond-valence calculations, we write the ideal and simplified formulae of veblenite as the sum of the cation and anion components: $K_2\square_2Na$ $(Fe_5^{2+}Fe_4^{3+}Mn_7^{2+}\square)Nb_3Ti(Si_2O_7)_2$ $(Si_8O_{22})_2O_6$ $(OH)_{10}(H_2O)_3$ and (K,Ba,□)$_3$(□,Na)$_2$ $(Fe^{2+},Fe^{3+},Mn^{2+})_{17}(Nb,Ti)_4$ $(Si_2O_7)_2(Si_8O_{22})_2O_6$ $(OH)_{10}(H_2O)_3$, respectively, $Z = 1$. The validity of the ideal formula is supported by the good agreement between the total charges for cations in the ideal and empirical formulae: 3^+ $[K_2\square_2Na]$ + 36^+ $[Fe_5^{2+}Fe_4^{3+}Mn_7^{2+}\square]$ + 19^+ $[Nb_3Ti]$ = 58^+ *vs.* 3^+ $[\square_{2.48}K_{1.25}Na_{0.72}Ba_{0.28}$ $Ca_{0.17}Cs_{0.07}Sr_{0.03}]$ + 36.81^+ $[(Mn_{5.97}^{2+}Fe_{5.32}^{2+}Fe_{4.13}^{3+}$ $Ca_{0.70}\square_{0.66}Zn_{0.15}Mg_{0.07})]$ + 18.73^+ $[(Nb_{2.90}Ti_{0.93}Fe_{0.17}^{2+})]$ = 58.54^+.

The general structural formula of veblenite

Above, we wrote the ideal formulae of veblenite based on the sum of the cation and anion

components: $K_2\square_2Na(Fe^{2+}_5Fe^{3+}_4Mn^{2+}_7\square)Nb_3Ti(Si_2O_7)_2(Si_8O_{22})_2O_6(OH)_{10}(H_2O)_3$, Z = 1. The structural formula has the form $A_1A_2B_2M_{17}D_4(Si_2O_7)_2(Si_8O_{22})_2X^O_{D4}X^P_{D2}X^O_{A10}W_8$ where A and B are interstitial cations; M and D are cations of the O and H sheets; X^O are anions of the O sheet; X^P_D are common anions for the D cations and from two adjacent HOH layers; and W are H_2O groups in the wide channels. The structural formula obtained from chemical analysis (Table 2) is therefore $(K_{0.53}Ba_{0.28}Sr_{0.03}\square_{0.16})_{\Sigma1}(K_{0.72}Cs_{0.07}\square_{1.21})_{\Sigma2}(Na_{0.72}Ca_{0.18}\square_{1.10})_{\Sigma2}(Fe^{2+}_{5.32}Fe^{3+}_{4.13}Mn^{2+}_{5.97}Ca_{0.70}Zn_{0.15}Mg_{0.07}\square_{0.66})_{\Sigma17}(Nb_{2.90}Ti_{0.93}Fe^{3+}_{0.17})_{\Sigma4}(Si_2O_7)_2(Si_{7.80}Al_{0.20}O_{22})_2O_6(OH_{9.78}F_{0.22})_{\Sigma10}(H_2O)_2[(H_2O)_{1.23}\square_{2.77}]_{\Sigma4}$. The ideal formula of veblenite, $K_2\square_2Na(Fe^{2+}_5Fe^{3+}_4Mn^{2+}_7\square)Nb_3Ti(Si_2O_7)_2(Si_8O_{22})_2O_6(OH)_{10}(H_2O)_3$, requires Nb_2O_5 12.76, TiO_2 2.56, SiO_2 38.46, Fe_2O_3 10.22, MnO 15.89, FeO 11.50, K_2O 3.01, Na_2O 0.99, H_2O 4.61; total 100.00 wt.%. The simplified formula of veblenite is $(K,Ba,\square)_3(\square,Na)_2(Fe^{2+},Fe^{3+},Mn^{2+})_{17}(Nb,Ti)_4(Si_2O_7)_2(Si_8O_{22})_2O_6(OH)_{10}(H_2O)_3$.

Summary

Veblenite is a new (Nb,Ti)-silicate mineral with a new structure that has no natural or synthetic analogues. It is triclinic: space group $P\bar{1}$, *a* 5.3761(3), *b* 27.5062(11), *c* 18.6972(9) Å, α 140.301(3), β 93.033(3), γ 95.664(3)°, *V* = 1720.96(14) Å^3. The structural unit of veblenite is an HOH layer. Dominant cations in the O sheet are $(Fe^{2+} + Fe^{3+}) > Mn^{2+}$, with $Fe^{2+} > Fe^{3+}$. The H sheet is composed of (Nb,Ti) octahedra, Si_2O_7 groups and the veblenite Si_8O_{22} ribbon, a new type of Si−O ribbon. In the structure, the HOH layers connect *via* common anions of (Nb,Ti) octahedra. In the interstitial space between two HOH layers, K and Na atoms and H_2O groups constitute the **I** block.

We write the ideal and simplified formulae of veblenite (*Z* = 1) as $K_2\square_2Na(Fe^{2+}_5Fe^{3+}_4Mn^{2+}_7\square)Nb_3Ti(Si_2O_7)_2(Si_8O_{22})_2O_6(OH)_{10}(H_2O)_3$ and $(K,Ba,\square)_3(\square,Na)_2(Fe^{2+},Fe^{3+},Mn^{2+})_{17}(Nb,Ti)_4(Si_2O_7)_2(Si_8O_{22})_2O_6(OH)_{10}(H_2O)_3$, respectively. Aspects of the crystal chemistry of veblenite will be considered in a later paper.

Acknowledgements

We thank Jeffrey Post and Ian Grey for reviewing the manuscript. FCH was supported by a Canada Research Chair in Crystallography and Mineralogy, by Discovery and Major Installation grants from the Natural Sciences and Engineering Research Council of Canada, and by Innovation Grants from the Canada Foundation for Innovation. FC also thanks Frank Hawthorne for supporting a visiting research period at Winnipeg.

References

Brown, I.D. (1981) The bond-valence method: an empirical approach to chemical structure and bonding. Pp. 1−30 in: *Structure and Bonding in Crystals II* (M. O'Keeffe and A. Navrotsky, editors). Academic Press, New York.

Cámara, F. and Sokolova, E. (2007) From structure topology to chemical composition. VI. Titanium silicates: the crystal structure and crystal chemistry of bornemanite, a group-III Ti-disilicate mineral. *Mineralogical Magazine*, **71**, 593−610.

Cámara, F. and Sokolova, E. (2009) From structure topology to chemical composition. X. Titanium silicates: the crystal structure and crystal chemistry of nechelyustovite, a group III Ti-disilicate mineral. *Mineralogical Magazine*, **73**, 887−897.

Cámara, F., Sokolova, E., Abdu, Y. and Hawthorne, F.C. (2010) The crystal structures of niobophyllite, kupletskite-(Cs) and Sn-rich astrophyllite; revisions to the crystal chemistry of the astrophyllite-group minerals. *The Canadian Mineralogist*, **48**, 1−16.

Cámara, F., Sokolova, E. and Hawthorne, F.C. (2012) Kazanskyite, $Ba\square TiNbNa_3Ti(Si_2O_7)_2O_2(OH)_2(H_2O)_4$, a Group-III Ti-disilicate mineral from the Khibiny alkaline massif, Kola Peninsula, Russia: description and crystal structure. *Mineralogical Magazine*, **76**, 473−492.

Ercit, T.S., Cooper, M.A. and Hawthorne, F.C. (1998) The crystal structure of vuonnemite, $Na_{11}Ti^{4+}Nb_2(Si_2O_7)_2(PO_4)_2O_3(F,OH)$, a phosphate-bearing sorosilicate of the lomonosovite group. *The Canadian Mineralogist*, **36**, 1311−1320.

Ferraris, G. (2008) Modular structures − the paradigmatic case of the heterophyllosilicates. *Zeitschrift für Kristallographie*, **223**, 76−84.

Ferraris, G., Ivaldi, G., Khomyakov, A.P., Soboleva, S.V., Belluso, E. and Pavese, A. (1996) Nafertisite, a layer titanosilicate member of a polysomatic series including mica. *European Journal of Mineralogy*, **8**, 241−249.

Hawthorne, F.C. (2012) Bond topology and structure-generating functions: graph-thoretic prediction of chemical composition and structure in polysomatic T−O−T (biopyribole) and H−O−H structures. *Mineralogical Magazine*, **76**, 1053−1080.

Hong, W. and Fu, P. (1982) Jinshajiangite, a new Ba-Mn-Fe-Ti-bearing silicate mineral. *Geochemistry*

(China), **1**, 458–464.

Khomyakov, A.P., Ferraris, G., Ivaldi, G., Nechelyustov, G.N. and Soboleva, S.V. (1995) Nafertisite, $Na_3(Fe^{2+},Fe^{3+})_6[Ti_2Si_{12}O_{34}](O,OH)_7{\cdot}2H_2O$, a new mineral with a new type of banded silicate radical. *Zapiski Vserossiyskogo Mineralogicheskogo Obshchestva*, **124**, 101–107 (in Russian).

Nickel, E.H., Rowland, J.F. and Charette, D.J. (1964) Niobophyllite-the niobium analogue of astrophyllite; a new mineral from Seal Lake, Labrador. *The Canadian Mineralogist*, **8**, 40–52.

Pouchou, J.L. and Pichoir, F. (1985) 'PAP' φ(ρZ) procedure for improved quantitative microanalysis. Pp. 104–106 in: *Microbeam Analysis* (J.T. Armstrong, editor). San Francisco Press, San Francisco, California, USA.

Rowe, R. (2009) New statistical calibration approach for Bruker AXS D8 Discover microdiffractometer with Hi-Star detector using GADDS software, *ICDD Powder diffraction Journal*, **24**, 263–271.

Shannon, R.D. (1976) Revised effective ionic radii and systematic studies of interatomic distances in halides and chalcogenides. *Acta Crystallographica*, **A32**, 751–767.

Sheldrick, G.M. (2008) A short history of SHELX. *Acta Crystallographica*, **A64**, 112–122.

Sokolova, E. (2006) From structure topology to chemical composition. I. Structural hierarchy and stereochemistry in titanium disilicate minerals. *The Canadian Mineralogist*, **44**, 1273–1330.

Sokolova, E. (2012) Further developments in the structure topology of the astrophyllite-group minerals. *Mineralogical Magazine*, **76**, 863–882.

Sokolova, E. and Hawthorne, F.C. (2004) The crystal chemistry of epistolite. *The Canadian Mineralogist*, **42**, 797–806.

Sokolova, E., Cámara, F., Hawthorne, F.C. and Abdu, Y. (2009) From structure topology to chemical composition. VII. Titanium silicates: the crystal structure and crystal chemistry of jinshajiangite. *European Journal of Mineralogy*, **21**, 871–883.

Wilson, A.J.C. (editor) (1992) *International Tables for Crystallography. Volume C: Mathematical, Physical and Chemical*. Kluwer Academic Publishers, Dordrecht, The Netherlands.